Biosensors and Bioelectronics 24 (2009) 2470–2474

Contents lists available at ScienceDirect

Biosensors and Bioelectronics

journal homepage: www.elsevier.com/locate/bios

Cathodic detection of H_2O_2 based on nanopyramidal gold surface with enhanced electron transfer of myoglobin

Peipei Xia, Haiqing Liu, Yang Tian*

Department of Chemistry, Tongji University, Siping Road 1239, Shanghai 200092, PR China

ARTICLE INFO

Article history:
Received 26 September 2008
Received in revised form 2 December 2008
Accepted 17 December 2008
Available online 25 December 2008

Keywords:
Direct electron transfer
Pyramidal gold nanostructures
Myoglobin (Mb)
Hydrogen peroxide (H_2O_2)
Biosensor

ABSTRACT

Direct and reversible electron transfer of myoglobin (Mb), for the first time, is achieved at nanopyramidal gold surface, which was fabricated by one-step electrodeposition, with redox formal potential of 0.21 ± 0.01 V (vs. Ag/AgCl) and an apparent heterogeneous electron-transfer rate constant (k_s) of $1.6 \pm 0.2\ s^{-1}$. Electrochemical investigation indicates that Mb is stably confined on the nanopyramidal gold surface and maintains electrocatalytic activity toward hydrogen peroxide (H_2O_2). The facilitated electron transfer combined with the intrinsic catalytical activity of Mb substantially construct the third-generation biosensor for H_2O_2. The positive redox potential of Mb at the nanostructured gold electrode gives a strong basis for determination of H_2O_2 with high selectivity. Besides this advantage, the present biosensor also exhibits quick response time, broad linear range, and good sensitivity. The dynamic detection linear range is from 1 μM to 1.4 mM with a detection limit of 0.5 μM at 3σ. The striking analytical performance of the present biosensor, as well as the biocompatibility of gold nanostructures provided a potential for continuous, on-line detection of H_2O_2 in the biological system.

1. Introduction

Determination of hydrogen peroxide (H_2O_2) with high selectivity and sensitivity is of great importance, because H_2O_2 is cytoxic to cellular life and is an indicator of oxidative stress (Yorek, 2003) and a product of several biological, enzyme-catalyzed reactions (Thome-Duret et al., 1996; You et al., 2003). It is also important in terms of developing biosensors for determining H_2O_2 in food, pharmaceutical, clinical, industrial and environmental analyses (Wang et al., 1993; Kulys et al., 1993). A series of techniques were employed for H_2O_2 analysis, such as titrimetry (Weber et al., 2004), photometry (Vasily et al., 1995), chemiluminescence (Sakai et al., 2008), and high performance liquid chromatography (Schaeffer et al., 2008). Amperometric biosensors have received considerable interests due to their high sensitivity, real-time monitoring, and low-cost. Numerous electrochemical sensors based on the use of different chemicals, such as Pt (Karam and Halaoui, 2008), I^- (Miah and Ohsaka, 2006), (3-mercaptopropyl)trimethoxysilane (Shankaran et al., 2003), Prussian Blue (De Mattos et al., 2003; Garjonyte and Malinauskas, 1999), cyclopentadienylnickel(II)thiolato Schiffbase (Morrin et al., 2004), tris(2,2′-bipyridil)copper(II) chloride complex (Sotomayor et al., 2003), hemoglobin (Hb) (Gu et al., 2001), myoglobin (Mb) (Dai et al., 2004a), manganese hexacyanoferrate (Eftekhari, 2001), horseradish peroxidase (HRP) (Kong et al., 2003; Karyakin et al., 2000; Kenausis et al., 1997), etc., have been used for the determination of H_2O_2. Because of the favorable selectivity of the enzymes, the third-generation biosensors based on the direct electron transfer of enzymes has been attracted much more attention.

In order to construct the third-generation biosensors, the first step is to realize direct electron transfer of enzymes. The approach to direct electron transfer requires interfaces that exhibit fast electron-transfer kinetics with biocompatibility, since direct contact between redox enzymes and electrode surfaces leads to significant structural and/or functional changes of enzymes (Lu et al., 2006a). In order to attain original conformations and bioactivities of the enzyme, the modification of the electrode (which can increase electron transfer between the enzyme and the electrode) has been very popular in recent 30 years (Bistolas et al., 2005; Huang et al., 2002; Lu et al., 2006b; Liu et al., 2005).

With the development of nanomaterials, gold nanoparticles (GNPs), which have been known for 2500 years, are the subject of an exponentially increasing number of publications, because of their fascinating research and promises for optical, electronic, magnetic, catalytic, and biomedical applications (Kim et al., 2002, 2004; Zhang et al., 2006a; Millstone et al., 2005; Tian and Tatsuma, 2005, 2004). More importantly, additional reasons for the present excitement in GNPs research are the complete biocompatibility and stability of GNPs. Actually, direct contact between naked GNPs and proteins is common in histochemistry, where it has been demonstrated that electrostatically bound GNPs–protein conjugates typically retain biological activity. Indeed, Crumbliss' group

* Corresponding author. Tel.: +86 21 65987075; fax: +86 21 65982287.
E-mail address: yangtian@mail.tongji.edu.cn (Y. Tian).

0956-5663/$ – see front matter © 2008 Elsevier B.V. All rights reserved.
doi:10.1016/j.bios.2008.12.029

found that several enzymes could maintain their biocatalytical and electrochemical activities when immobilized on GNPs (Crumbliss et al., 1993). Among various methods for preparation of protein films with GNPs, the layer-by-layer self-assembly technique, which is based on the alternate adsorption of oppositely charged species from their solutions, has been developed into a general approach for immobilization of Mb on GNPs (Zhang and Hu, 2007a,b; Zhang et al., 2006b). These existing studies give support to the engineering feasibility of preparing multilayer films of GNPs/protein nanocomposites.

In our previous work, nanopyramidal gold surface was fabricated on polycrystalline gold substrates through electrochemical overpotential deposition (Tian et al., 2006). Direct and reversible electron transfer of Mb for the first time was realized at nanopyramidal gold surface with redox formal potential of 0.21 ± 0.01 V (vs. Ag/AgCl) without any mediators or promoters. Meanwhile, Mb processed the inherent enzymatic activity after being immobilized on nanopyramidal gold surfaces. Consequently, the Mb-pyramidal gold nanocomposites were successfully fabricated for determination of H_2O_2 with high selectivity and broad linear range.

2. Experimental

2.1. Reagents

Hydrogen tetrachloroaurate(III) ($HAuCl_4$) trihydrate was purchased from Aldrich (St. Louis, MO) and used as supplied. Horse heart myoglobin (MW 17,800) was purchased from Sigma and used without further purification. Phosphate buffer solution (PBS, 10 mM) was prepared by mixed stock standard K_2HPO_4 and KH_2PO_4 solutions and pH of PBS was adjusted by pH meter. Other reagents were of analytical grade and used as received. All the solutions were prepared with doubly distilled water and were deaerated with high purity nitrogen for 30 min before experiments.

2.2. Preparation and modification of pyramidal gold surface

Gold electrodes (1.6 mm in diameter) purchased from Bioanalytical Systems Inc. (BAS, West Lafayette, IN) were polished with emery paper (#2000) and aqueous slurries of successively finer alumina powder (down to 0.05 μm) on a polishing microcloth, sonicated in water for 10 min and finally rinsed with water. The electrodes were then electropolished by potential cycling in 0.05 M H_2SO_4 solution in the potential range of −0.2 to 1.5 V vs. Ag/AgCl at a scan rate of 10 V s^{-1} until the typical cyclic voltammogram characteristic of a clean Au electrode was obtained. Pyramidal gold nanostructure was electrodeposited from aqueous solutions of 0.1 M $HClO_4$ containing 40 mM $HAuCl_4$, at −0.08 V vs. Ag/AgCl for 2 min. Pyramidal gold electrode was modified with Mb by immersing the electrodes into PBS (pH 7.2) of Mb (0.1 mM) for over one night at 4 °C in refrigerator. (The inherent enzymatic activity of Mb solution stored in refrigerator was monitored by UV–vis absorption spectroscopy. No obvious UV–vis spectrum change of Mb solution was observed up to 30 days.) Hereafter, the Mb modified nanopyramidal gold electrode will be referred to as Au-NP/Mb. After electrochemical experiments, the modified electrodes were rinsed thoroughly with doubly distilled water and kept in PBS at 4 °C.

2.3. Apparatus and measurements

A CHI 660A and CHI 832 electrochemical work station (CH Instruments, USA) was employed in all electrochemical measurements, which were carried out with a conventional two compartment three-electrode electrochemical cell. The reference electrode was a KCl-saturated Ag/AgCl electrode, while the auxilliary electrode was a platinum wire. A about 50-nm-thick Au film was sputtered onto the clean ITO-coated glass with a high-vacuum metal sputter coater EMS-550X (EMS Inc., USA). An atomic force microscope SPA-300HV (Seiko Instruments Inc., Japan) was employed to record the images of the nanostructured gold surfaces. The UV–vis absorption spectrum of the solution was recorded by an Agilent 8453 UV–vis spectrophotometer (Agilent Instruments). All of the electrochemical measurements were performed at laboratory temperature (25 ± 1 °C).

3. Results and discussion

3.1. Surface properties of gold nanopyramids

The morphology of the nanopyramidal gold surface was characterized by atomic force spectroscopy (AFM) as shown in Fig. 1. The background—a sputtered gold surface shows a spherical image with diameter of around 50 nm (Fig. 1a). As Fig. 1b depicts, nanopyramidal structures with 50–200 nm edge length of bottom and several hundreds nanometers height were obtained at a potential of −0.08 V vs. Ag/AgCl in a 40 mM $HAuCl_4$ solution.

To characterize electrochemical properties of the nanopyramidal gold surface, cyclic voltammetry of an electron-transfer indicators such as $Fe(CN)_6^{3-/4-}$ was studied at the nanopyramidal gold electrode, compared with that at sputtered gold substrate. As depicted in Fig. 2a, redox behavior of $Fe(CN)_6^{3-/4-}$ was obtained at sputtered gold substrate with a peak-to-peak separation (ΔE_p) of about 125 mV at a potential scan rate of 100 mV s^{-1}. However, at the nanopyramidal gold surface (Fig. 2b), a pair of well-defined redox peaks was observed with a ΔE_p of ∼ 60 mV and a near unity of anodic-to-cathodic peak current ration (I_p^a/I_p^c), which is a typical characteristic of the reversible process of the redox species in solution phase. The standard electron-transfer rate constant (k^0) was calculated by Nicholson theory (Nicholson, 1965) to be 0.23 cm s^{-1} at nanopyramidal (Fig. 2b) gold surface, which is much greater than that obtained at sputtered gold of about 0.06 cm s^{-1}. It indicates that electron transfer is greatly facilitated at the nanopyramidal gold surface, which was further confirmed by electrochemical impedance spectroscopy (EIS), as demonstrated in Fig. 3. The charge-transfer resistance (R_{ct}) of the $Fe(CN)_6^{3-/4-}$ redox couple is near 116 Ω at the sputtered gold substrate (Fig. 3a), but it decreases to 16 Ω at nanopyramidal (Fig. 3b) gold surface. The decrease in the charge-transfer resistance at the nanopyramidal gold surface,

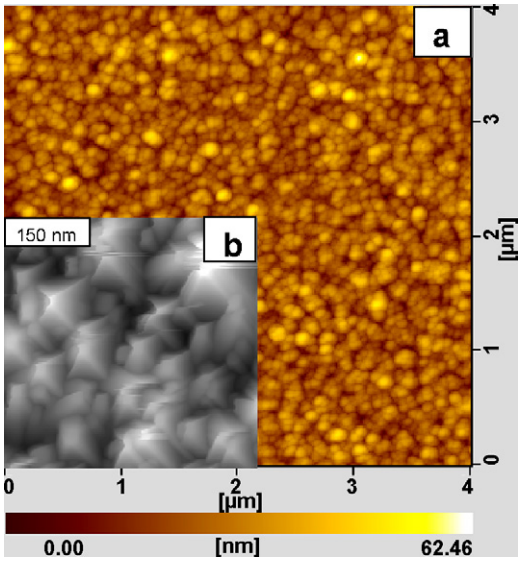

Fig. 1. AFM images of (a) a sputtered gold surface and (b) pyramidal gold surface. Similar images were observed when different spots were scanned.

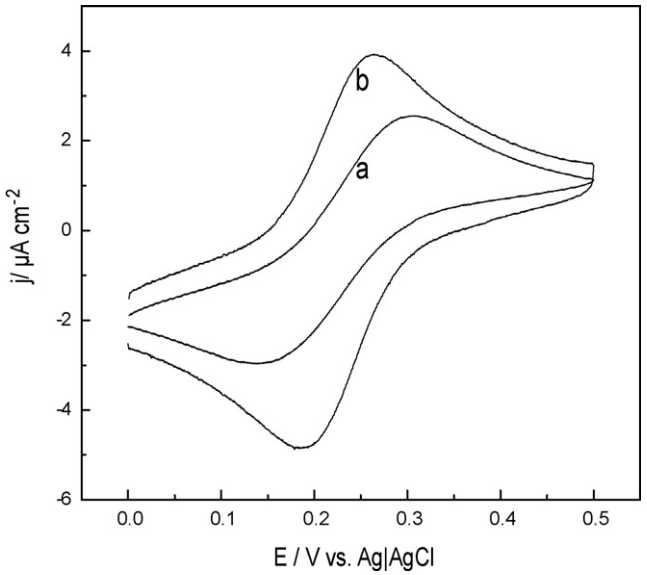

Fig. 2. CVs obtained at (a) sputtered gold substrate and (b) nanopyramidal gold nanostructured electrodes in 0.1 M KCl solution containing 1 mM $[Fe(CN)_6]^{3-/4-}$. Potential scan rate: 100 mV s^{-1}.

indicates that gold nanopyramids intrinsically enhance the electron transfer of the $Fe(CN)_6^{3-/4-}$ redox couple.

3.2. Electrochemistry of Mb on the nanopyramidal gold surface

Fig. 4 shows typical cyclic voltammograms (CVs) obtained at bare gold substrate (a), Au/Mb (b), gold nanopyramids (c), and Au-NP/Mb (d) in 10 mM PBS (pH 7.2) solution at the potential scan rate of 100 mV s^{-1}. Only charge currents were obtained at the bare gold (a) and nanopyramidal (c) gold surfaces. However, a pair of well-defined redox peaks was observed at the Au-NP/Mb electrode, although no response of Mb was observed at bare gold substrate (b), suggesting that direct electron transfer was only achieved between Mb and nanopyramidal gold electrode (Fig. 4d). The formal potential ($E^{0\prime} = (E_{p,a} + E_{p,c})/2$) of Au-NP/Mb was estimated to be 0.21 ± 0.01 V (vs. Ag/AgCl).

CVs of Au-NP/Mb in PBS (pH 7.2) at various scan rates were also obtained (Supporting Information, Fig. S1). We found that both the

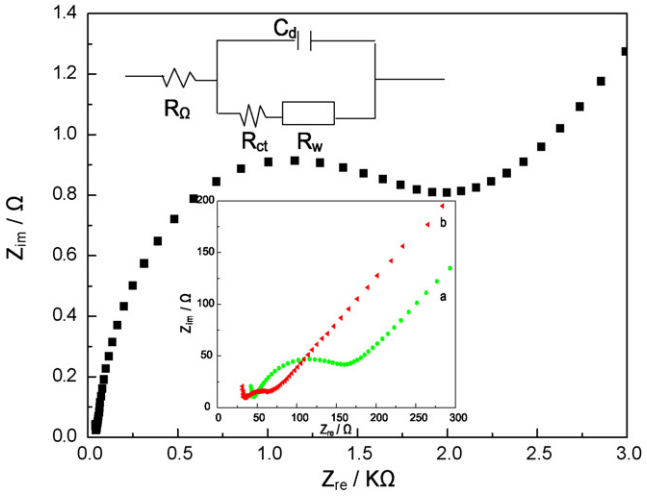

Fig. 3. Nyquist plots obtained at (a) sputtered gold substrate, (b) Au-NP and (c) Au-NP/Mb electrodes in 0.1 M KCl solution containing 1 mM $[Fe(CN)_6]^{3-/4-}$. EIS conditions: potential, 0.28 V; alternative voltage, 5 mV; frequency range, 0.1–10^5 Hz.

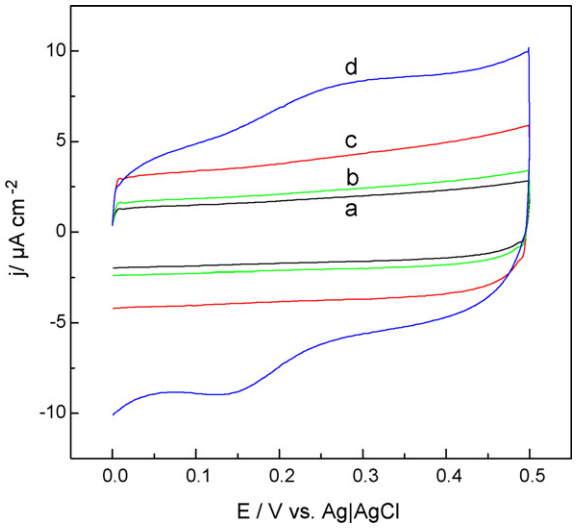

Fig. 4. CVs obtained at (a) bare Au, (b) Au/Mb, (c) Au-NP and (d) Au-NP/Mb electrodes in 10 mM PBS (pH 7.2). Potential scan rate: 100 mV s^{-1}.

anodic and cathodic peak currents (I_p^a and $_p^c$) vary linearly with the potential scan rate (v) in the range of 10–300 mV s^{-1} (the inset in Fig. S1), indicating a surface-controlled process. In addition, the CVs remained essentially unchanged upon consecutive potential scanning up to 100 cycles at a sweep rate of 20 mV s^{-1}, indicating that Mb is stably confined on nanopyramidal gold surfaces. According to Laviron's procedure (Laviron, 1979), from the potential scan rate dependence of the anodic and cathodic peak potentials, the relevant kinetic parameters of the electrode reaction, that is, the rate constant of the electrochemical process (k_s) and the anodic and cathodic transfer coefficients (α_a and α_c), were estimated: $k_s = 1.6 \pm 0.2$ s^{-1}, $\alpha_a = 0.55 \pm 0.06$, $\alpha_c = 0.45 \pm 0.06$ at nanopyramidal gold surface.

The adsorbed behavior of Mb and its surface coverage immobilized on the nanostructured gold surfaces could also be followed by EIS. Fig. 3c shows Nyquist plot obtained at Au-NP/Mb electrode. The charge-transfer resistance of Mb-immobilized nanopyramidal gold electrode increased by a factor of $\sim 10^2$, compared with that obtained at bare nanopyramidal gold surfaces as shown in Fig. 3b. It confirmed again that Mb adsorbed onto nanopyramidal gold surface and inhibited the electrochemical communication between the electron-transfer indicator ($Fe(CN)_6^{3-/4-}$) and the nanopyramidal gold electrode. The surface coverage (θ) of Mb confined at the nanopyramidal gold surface can be derived from the equation $\theta = 1 - R_{ct}/R_{ct}^{Mb}$, where R_{ct} is the charge-transfer resistance of the nanostructured gold surfaces, and R_{ct}^{Mb} is the corresponding resistance of Mb-immobilized surfaces. The surface coverage of Mb confined at nanopyramidal surfaces was estimated to be 99.2%. The average surface adsorption amount of electroactive Mb (Γ, mol cm^{-2}) was also estimated from the charge integration of the reduction peak of the cyclic voltammogram of Au-NP/Mb, using the formula of $\Gamma = Q/nFA$, where Q is the charge (C), n is the number of transfer electrons, F is the Faraday constant, and A is the surface area of the Au-NP electrode (cm^{-2}). The average surface amount of electroactive Mb was calculated to be $(3.1 \pm 0.14) \times 10^{-11}$ mol cm^{-2}. Standard deviations are given from at least six electrodes.

3.3. Electrocatalytic activity of Mb confined on gold nanopyramids

As demonstrated above, nanopyramidal surface facilitates the electron transfer of Mb itself, and Mb is stably confined on the gold nanostructures. This result formed a strong basis for the develop-

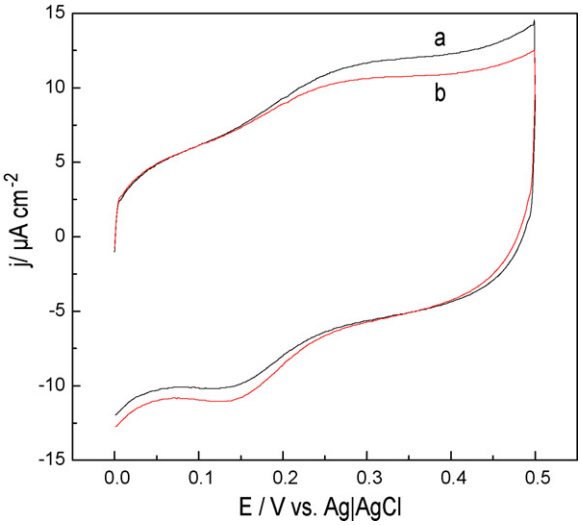

Fig. 5. CVs obtained at Au-NP/Mb electrode in the absence (a) and presence (b) of 10 μM H_2O_2 in 10 mM PBS (pH 7.2). Potential scan rate: 100 mV/s.

ment of a third-generation biosensor for H_2O_2 because the heme has been well documented as the active site for the catalysis to the reduction of H_2O_2 (Zhao et al., 2005; Dai et al., 2004b). The electrocatalytic activity of electrode toward H_2O_2 was investigated by CV. Fig. 5 displays CVs obtained at Au-NP/Mb electrode in the absence (a) and presence (b) of 10 μM H_2O_2 in 10 mM PBS (pH 7.2). The addition of 10 μM H_2O_2 to 10 mM PBS (pH 7.2) obviously increases the cathodic current and decreases the anodic currents of the Mb confined on nanopyramidal gold electrodes, indicating the good electrocatalytic activity of the immobilized Mb for the reduction of H_2O_2.

3.4. Analytical performance of the H_2O_2 biosensor

The typical amperometric responses of Au-NP/Mb to successive concentration changes of H_2O_2 were examined at the applied potential of 50 mV, and the corresponding current–time responses are shown in Fig. 6. Well-defined steady-state current responses were obtained at nanopyramidal gold electrode, and the currents increased stepwise with successive additions of H_2O_2. The calibration plots are shown in the inset of Fig. 6. The steady-state currents at nanopyramidal gold electrode were proportional to H_2O_2 in the

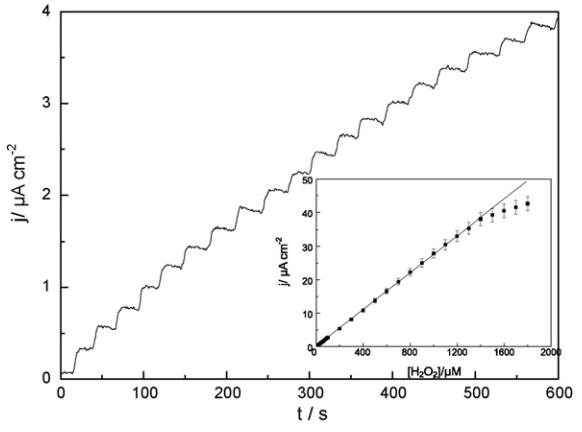

Fig. 6. Typical steady-state amperometric responses obtained at Au-NP/Mb electrodes at the applied potential of 50 mV in 10 mM PBS solution (pH 7.2) upon the successive addition of 10 μM H_2O_2. The inset is a plot of catalytic peak current against the concentration of H_2O_2.

examined range of 1 μM–1.4 mM with a correlation coefficient of 0.999 (n = 10). The linear range is wider than those obtained on Mb–gold nanoparticles surfaces (Zhang et al., 2006b; Yang et al., 2006; Zhang and Oyama, 2005; Liu and Ju, 2003; Cao et al., 2008). The sensitivity of Au-NP/Mb was estimated to be 33 μA/(cm^2 mM). The detection limit was evaluated on the basis of a signal-to-noise ratio of 3:1 and calculated to be 0.5 μM at nanopyramidal gold surface. The response time of the sensor was measured as the time to reach 95% of the maximum change in response to a step injection of H_2O_2 and was found to be less than 8 s.

When the concentration of H_2O_2 is higher than 1.4 mM, a response plateau is observed, showing the characteristics of the Michaelis–Menten kinetic mechanism. The apparent Michaelis–Menten constant (K_M^{app}), which gives an indication of the enzyme–substrate kinetics, can be obtained from the electrochemical version of the Lineweaver–Burk equation (Kamin and Wilson, 1980):

$$\frac{1}{I_{ss}} = \frac{1}{I_{max}} + \frac{K_M^{app}}{I_{max}C}$$

where I_{SS} is the steady-state current after the addition of substrate, which can be obtained from amperometric experiments, I_{max} is the maximum current under saturated substrate condition and C is the bulk concentrate of the substrate. K_M^{app} is the apparent Michaelis–Menten constant and a characteristic parameter of the enzyme–substrate kinetics. The value of the apparent Michaelis–Menten constant (K_M^{app}) can be calculated from the slope (K_M^{app}/I_{max}) and the intercept ($1/I_{max}$) for the plot of the reciprocals of the steady-state current (I_{SS}) vs. H_2O_2 concentration (C). In this work, the K_M^{app} value for the Au-NP/Mb electrode is estimated to be 0.27 mM, smaller than that of Hb/nano-Au/L-cys/nano-Au/nano-Pt-CHIT electrode (Yang et al., 2008) and Hb/Au–ZrP/chitosan/GCE (Feng et al., 2005a). The low value of K_M^{app} indicates that Mb immobilized on the Au-NP/Mb electrode retains its bioactivity and has a high biological affinity to H_2O_2.

For the stability test, the 100 continuous cyclic scans was carried out in the potential range from 0 to 0.5 V with a 50 mV/s scan rate, only 5% decrease of the initial response is observed. On the other hand, the storage stability of the proposed biosensor was also studied. When not in use, the electrode was suspended above 10 mM phosphate buffer at 4 °C in a refrigerator. The cathodic responses for H_2O_2 were recorded four times each day, and the current responses were found to be constant for at least 2 weeks. The stability can be attributed to the compatibility of the Au-NP, and it may also be due to the fact that Au-NP was biocompatible so that Mb was attached firmly onto the surface. In addition, with the successive addition of 10 μM H_2O_2 for 10 times, we have found that the deviation of the current responses of 10 sensors prepared with the same method did not exceed 5% (RSD).

In addition, at the applied potential of 0.05 V, the common interferences like AA, UA, DA, DOPAC, glucose, L-cysteine, NO_2^-, NO_3^-, and SO_3^{2-} were negligible (< 1%) at Au-NP/Mb electrode, indicating that the present H_2O_2 biosensor showed high selectivity.

4. Conclusions

A facile, but effective way to realize direct electron transfer of Mb was developed at nanopyramidal gold surface without any mediators or promoters. The redox formal potential of Mb was obtained to be 0.21 ± 0.01 V (vs. Ag/AgCl) at the nanostructured gold surface and an apparent heterogeneous electron-transfer rate constant (k_s) was calculated to be 1.6 ± 0.2 s^{-1}. Experimental results suggested that Mb was stably confined on the nanopyramidal gold surface and processed electrocatalytic activity toward H_2O_2. The facilitated electron transfer combined with the intrinsic catalytical activity

of Mb substantially constructed the third-generation biosensor for H_2O_2. Besides high selectivity, the present third-generation biosensor also displayed wide linear range, low detection limit, fast response, and good long-term stability for the detection of H_2O_2.

Acknowledgements

This work was financially supported by the Program for New Century Excellent Talents in University (NCET-06-0380) and the Scientific Research Foundation for the Returned Overseas Chinese Scholars from the Ministry of Education, China, and the Shanghai Pujiang Program (06PJ14090). Tongji University is also greatly acknowledged.

Appendix A. Supplementary data

Supplementary data associated with this article can be found, in the online version, at doi:10.1016/j.bios.2008.12.029.

References

Bistolas, N., Wollenberger, U., Jung, C., Scheller, F.W., 2005. Biosens. Bioelectron. 20, 2408–2423.
Cao, W., Wei, C.M., Hu, J.B., Li, Q.L., 2008. Electroanalysis 20, 1925–1931.
Crumbliss, A.L., Stonehuerner, J.G., Henkens, R.W., Zhao, J., O'Daly, J.P., 1993. Biosens. Bioelectron. 8, 331–337.
Dai, Z.H., Xu, X.X., Ju, H.X., 2004a. Anal. Biochem. 332, 23–31.
Dai, Z.H., Liu, S.Q., Ju, H.X., 2004b. Electrochim. Acta 49, 2139–2144.
De Mattos, I.L., Gorton, L., Ruzgas, T., 2003. Biosens. Bioelectron. 18, 193–200.
Eftekhari, A., 2001. Talanta 55, 395–402.
Feng, J.J., Xu, J.J., Chen, H.Y., 2005. J. Electroanal. Chem. 585, 44–50.
Huang, H., Hu, N.F., Zeng, Y.H., Zhou, G., 2002. Anal. Biochem. 308, 141–151.
Garjonyte, R., Malinauskas, A., 1999. Sens. Actuators, B 56, 93–97.
Gu, H.Y., Yu, A.M., Chen, H.Y., 2001. J. Electroanal. Chem. 516, 119–126.
Kamin, R.A., Wilson, G.S., 1980. Anal. Chem. 52, 1198–1205.
Karam, P., Halaoui, L.I., 2008. Anal. Chem. 80, 5441–5448.
Karyakin, A.A., Karyakina, E.E., Gorton, L., 2000. Anal. Chem. 72, 1720–1723.
Kenausis, G., Chen, Q., Heller, A., 1997. Anal. Chem. 69, 1054–1060.
Kim, F., Song, J.H., Yang, P., 2002. J. Am. Chem. Soc. 124, 14316–14317.
Kim, F., Connor, S., Song, H., Kuykendall, T., Yang, P., 2004. Angew. Chem. Int. Ed. 43, 3673–3677.
Kong, Y.T., Boopathi, M., Shim, Y.B., 2003. Biosens. Bioelectron. 42, 227–232.
Kulys, J., Wang, L., Maksimoviene, A., 1993. Anal. Chim. Acta 274, 53–58.
Laviron, E., 1979. J. Electroanal. Chem. 101, 19–28.
Liu, S.Q., Ju, H.X., 2003. Electroanalysis 15, 1488–1493.
Liu, Z.M., Yang, Y., Wang, H., Liu, Y.L., Shen, G.L., Yu, R.Q., 2005. Sens. Actuators, B 106, 394–400.
Lu, X.B., Hu, J.Q., Yao, X., Wang, Z.P., Li, J.H., 2006a. Biomacromolecules 7, 975–980.
Lu, X.B., Wen, Z.H., Li, J.H., 2006b. Biomaterials 27, 5740–5747.
Miah, M.R., Ohsaka, T., 2006. Anal. Chem. 78, 1200–1205.
Millstone, J.E., Park, S., Shuford, K.L., Qin, L., Schatz, G.C., Mirkin, C.A., 2005. J. Am. Chem. Soc. 127, 5312–5313.
Morrin, A., Moutloali, R.M., Killard, A.J., Smyth, M.R., Darkwa, J., Iwuoha, E.I., 2004. Talanta 64, 30–38.
Nicholson, R.S., 1965. Anal. Chem. 37, 1351–1355.
Sakai, S., Satow, T., Imakawa, K., Nagaoka, K., 2008. J. Dairy. Res. 75, 257–261.
Schaeffer, V., Patte-mensah, C., Eckertb, A., Mensah-Nyagana, A.G., 2008. Neuroscience 151, 758–770.
Shankaran, D.R., Iimura, K.I., Kato, T., 2003. Sens. Actuators, B 96, 523–526.
Sotomayor, M.D.P.T., Tanaka, A.A., Kubota, L.T., 2003. Electrochim. Acta 48, 855–865.
Thome-Duret, V., Reach, G., Gangnerau, M.N., Lemonnier, F., Klein, J.C., Zhang, Y., Hu, Y., Wilson, G.S., 1996. Anal. Chem. 68, 3822–3826.
Tian, Y., Tatsuma, T., 2005. J. Am. Chem. Soc. 127, 7632–7637.
Tian, Y., Tatsuma, T., 2004. Chem. Commun., 1810–1811.
Tian, Y., Liu, H.Q., Zhao, G.H., Tatsuma, T., 2006. J. Phys. Chem. B 110, 23478–23481.
Vasily, N.G., Marina, I.N., Alexander, D.R., 1995. Anal. Lett. 28, 2139–2148.
Wang, J., Lin, Y., Chen, L., 1993. Analyst 118, 277–280.
Weber, P.A., Thomas, J.E., Skinner, W.M., Smart, R.St.C., 2004. Appl. Geochem. 19, 687–694.
Yang, W.W., Li, Y.C., Bai, Y., Sun, C.Q., 2006. Sens. Actuator B: Chem. 115, 42–48.
Yang, G., Yuan, R., Chai, Y.Q., 2008. Colloids Surf. B 61, 93–100.
Yorek, M.A., 2003. Free Radic. Res. 37, 471–480.
You, T., Niwa, O., Tomita, M., Hirono, S., 2003. Anal. Chem. 75, 2080–2085.
Zhang, H., Hu, N.F., 2007a. Biosens. Bioelectron. 23, 393–399.
Zhang, H., Hu, N.F., 2007b. J. Phys. Chem. B 111, 10583–10590.
Zhang, J., Du, J., Han, B., Liu, Z., Jiang, T., Zhang, Z., 2006a. Angew. Chem. Int. Ed. 45, 1116–1119.
Zhang, H., Lu, H.Y., Hu, N.F., 2006b. J. Phys. Chem. B 110, 2171–2179.
Zhang, J.D., Oyama, M., 2005. J. Electroanal. Chem. 577, 273–279.
Zhao, G., Yin, Z., Zhang, L., Wei, X., 2005. Electrochem. Commun. 7, 256–260.